

Phase-transition induced magnetism modulation and logic implementation in NiFe/VO₂ heterostructure

Guodong Wei^{†,1,‡}, Xiaoyang Lin^{†,1,‡,}, Zhizhong Si[†], Dong Wang[§], Xinhe Wang^{†,□}, Kai Liu[△], Kaili Jiang[□], Zhaohao Wang[†], Na Lei[†], Yanxue Chen[§], Weisheng Zhao^{†,1,*}*

[†]Fert Beijing Research Institute, School of Electrical and Information Engineering & Beijing Advanced Innovation Center for Big Data and Brain Computing (BDBC),
Beihang University, Beijing 100191, China

¹Beihang-Goertek Joint Microelectronics Institute, Qingdao Research Institute,
Beihang University, Qingdao 266000, China

[§] School of Physics and State Key Laboratory of Crystal Materials, Shandong
University, Jinan 250100, China

[□] State Key Laboratory of Low-Dimensional Quantum Physics, Department of
Physics & Tsinghua-Foxconn Nanotechnology Research Center, Collaborative
Innovation Center of Quantum Matter, Tsinghua University, Beijing 100084, China

[△] School of Materials Science & Engineering, Tsinghua University, Beijing 100084,
China

[‡]These authors contributed equally.

*E-mail: XYLin@buaa.edu.cn (X.Y.L), weisheng.zhao@buaa.edu.cn (W.S.Z)

Abstract

With more degrees of freedom to manipulate information, multi-field control of magnetic and electronic properties may trigger various potential applications in spintronics and microelectronics. However, facile and efficient modulation strategies which can simultaneously respond to different stimuli are still highly desired. Here, the strongly correlated electron system VO_2 is introduced to realize efficient control of the magnetism in NiFe by phase-transition. The NiFe/ VO_2 bilayer heterostructure features appreciable modulations in the conductivity (10%), coercivity (60%), saturation magnetic strength (7%) and magnetic anisotropy (33.5%). Utilizing the multi-field modulation feature, programmable Boolean logic gates (AND, OR, NAND, NOR, XOR, NOT and NXOR) for high-speed and low-power data processing are demonstrated based on the heterostructure. Further analyses indicate that the interfacial strain coupling plays a crucial role in this modulation. As a demonstration of phase-transition spintronics, this work may pave the way for next-generation electronics in the post-Moore era.

Keywords: magnetism modulation; spin logic; phase-transition; multi-field; programmable

Efficient control of magnetism forms one of the key issues in next-generation spintronics, which features great potential in power consumption reduction and device miniaturization.¹⁻⁵ Many strategies have been used to achieve the goal, such as interfacial strain,^{6,7} charge transport,⁸ multiferroic coupling⁹ and even ion gating^{10,11}. Among these strategies, strain engineering which enables manipulation of spin, charge, and orbital degrees of freedom in thin film systems has attracted great interest.^{12,13} Progresses in strain engineering include reports of enhanced ferroelectric polarization¹⁴, high mobility strained transistors¹⁵, high-Curie temperature ferromagnetic properties¹⁶, and even enhanced superconductivity.¹⁷ Generally, epitaxial growth methods could introduce interfacial strain by lattice mismatch between film and substrates^{18,19}, but the

effect is static and non-tunable once the sample has been prepared. Adoption of flexible substrates enables dynamic strain engineering²⁰, although facing the challenge of miniaturization. Ferroelectric or piezoelectric ceramics can be used to generate dynamic strain by a converse piezoelectric effect.^{21,22} However, this manner is limited by the unsatisfactory coupling efficiency and the control manner is restricted to electric field.²³ In this regard, a strategy is highly desired to achieve high efficiency dynamic control of magnetism and meet the requirements of multi-field modulation.

Strongly correlated electron system is a kind of material that can respond to varieties of external stimuli, which is widely studied in many frontiers including high-temperature superconductors, two-dimensional electron gases and colossal magneto-resistive materials.²⁴ Functional states that are close in free energy can be yielded via multi-field inducing strategies including temperature variation, electric field gating or dimensionality changing in these materials.²⁵ In this sense, the collision and blending of strongly correlated electron systems and spintronic materials may revolutionize the strategy of magnetism modulation and pave a way for next-generation spintronics. In this work, we study the phase-transition induced magnetism modulation and programmable logic applications in NiFe/VO₂ heterostructures combining the strongly correlated electron systems with magnetic materials. The phase-transition of VO₂ can be triggered by temperature or red-light illumination (**Supplementary Fig. S1**). Appreciable modulations in conductivity (10%), coercivity (60%), saturation magnetic strength (7%) and uniaxial magnetic anisotropy (33.5%) have been achieved in this system. The interfacial magnetic anisotropy increases from 0.755 erg/cm² to 0.885 erg/cm², which also implies the feasibility of this strategy in spintronic device applications. Based on these modulation features, the heterostructures are also used to demonstrate multi-resistance states and implement basic logic functions with the assistance of light operation. Further analyses indicate that the interfacial strain coupling plays a crucial role in this modulation.

Heterostructure preparation and property modulation

The NiFe/VO₂ bilayer is used as a heterostructure system to explore the phase-transition induced multi-field modulation of magnetism. VO₂ is chosen as a representation of strongly correlated electron system, which exhibits complex property change as it transforms from a monoclinic (M1) insulator into a rutile (R) metal at the critical temperature around 340 K (**Figure 1a**).^{26–28} The phase-transition could be engineered by doping or strain to achieve different transition temperature and abruptness of the process.²⁹ In this work, TiO₂ substrates are chosen to get an epitaxial growth of VO₂ by pulsed laser deposition (PLD), and NiFe is deposited at room temperature by magnetron sputtering. **Figure 1b** gives the XRD result of the NiFe/VO₂ bilayer heterostructure samples. The (200) and (002) peaks of VO₂ can be detected on TiO₂ (100) and (001) substrates, respectively. The spectrum shows no distinct characteristic peak of NiFe, which means this layer is amorphous.

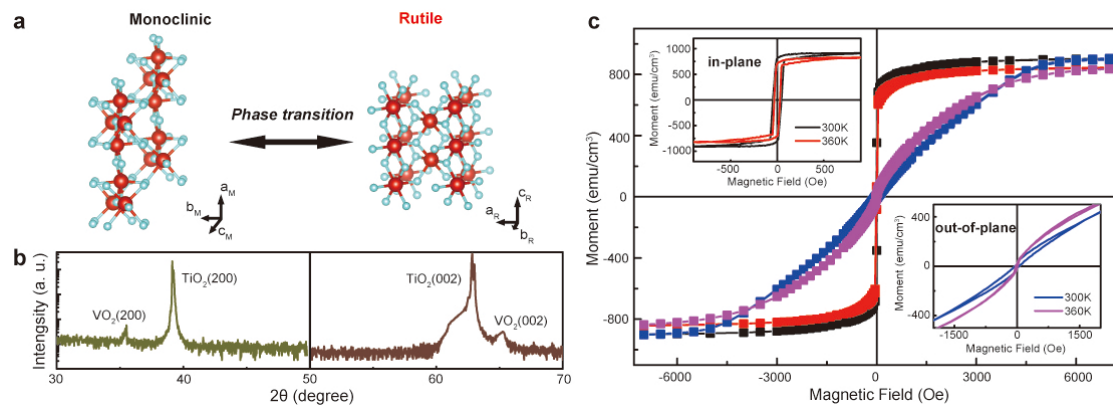


Figure 1 | Phase-transition of VO₂ and characterizations of the NiFe/VO₂ heterostructure. (a) The reversible phase-transition of VO₂ between monoclinic (M1) and rutile lattice structures. (b) XRD θ - 2θ scan of the NiFe/VO₂ heterostructure respectively grown on TiO₂ (100) and TiO₂ (001) substrates, suggesting an epitaxial growth of the VO₂ layer and an amorphous growth of the NiFe layer. (c) M - H hysteresis loops of NiFe (5 nm)/VO₂ (40 nm)/TiO₂ (100) sample measured at 300 and 360 K. Magnetic field was applied perpendicular and parallel to the surface. The insets give the scanning results of the small fields.

To investigate the magnetic properties modulated by phase-transition, hysteresis curves of NiFe (5 nm)/VO₂ (40 nm) sample grown on TiO₂ (100) substrate are measured

at 300 and 360 K in SQUID. As illustrated in **Figure 1c**, obvious anisotropy can be observed between the magnetic field applied in-plane and out-of-plane. After the phase-transition of VO₂, the saturation magnetization of the heterostructure system decreases from 898 emu/cm³ to 840 emu/cm³. The insets give the scanning results of the small fields, where a shrinking of coercive and saturation field can also be detected. Interestingly, the decrease is more obvious out-of-plane, making the squareness of the curve enhanced around zero field. The film exhibits an out-of-plane saturation field H_K of 4365 Oe at room temperature which drops about 136 Oe after the phase-transition. In the meantime, the coercive field drops from 72 Oe to 45 Oe reaching a change rate of 60%. Considering there are reports about the change in magnetic susceptibility of VO₂ during the phase transition,³⁰ temperature dependence of VO₂ magnetization has also been studied (**Supplementary Fig. S1c**). Excluding the effect of VO₂ single layer, this phase-transition induced magnetism modulation, which is distinguished from merely thermal effect (**Supplementary Fig. S2c**), shows great potential in spintronic applications like ultrafast magnetic storage.³¹

TABLE 1. Magnetic properties of SiO₂ (20 nm)/NiFe (t)/VO₂ (40 nm)/TiO₂

<i>Temperature</i>	<i>t</i>	<i>H_c</i>	<i>M_S</i>	<i>H_K</i> ^a	<i>K_u</i>	<i>K_i</i>
<i>K</i>	nm	<i>Oe</i>	emu/cm ³	Oe	erg/cm ³	erg/cm ²
300	5	72	898	4365	-3.55×10 ⁶	0.755
360	5	45	840	4229	-2.66×10 ⁶	0.885

^a H_K is obtained by extracting the field corresponding to 90% of measured moment out-of-plane

To further explore the modulation effect, magnetic parameters of the heterostructure at 300 and 360 K are summarized in **Table 1**. We analysis the hysteresis curves of the film in-plane and out-of-plane and get the uniaxial magnetic anisotropy K_u which increases from -3.55×10⁶ erg/cm³ to -2.66×10⁶ erg/cm³. To separate the bulk and interfacial contribution of the anisotropy, the relationship between K_u and NiFe thickness t can be written as $K_u=K_b-2\pi M_S^2+K_i/t$,³² where K_b is the bulk crystalline anisotropy, K_i is the interfacial anisotropy, and $-2\pi M_S^2$ is the demagnetizing field of a uniform sheet of NiFe. In this convention, $K_u < 0$ stands for an in-plane easy axis. The

increasing inclination therefore indicates the tendency to favour a perpendicular behaviour after the phase-transition.³³ Bulk crystalline anisotropy is negligible because the amorphous feature of the NiFe film. The interfacial magnetic anisotropy can then be calculated as $K_i=(K_u+2\pi M_S^2)t$, which increases from 0.755 erg/cm² to 0.885 erg/cm². These results indicate a possibility to realize interfacial perpendicular magnetic anisotropy enhancement in the heterostructure system which is highly desired in high-density non-volatile magnetic storage.³²

Device fabrication and multi-field control application

These appreciable effects in heterostructures may further enable emerging device applications with capability of multi-field modulation. As a demo, a phase-transition anisotropic magnetoresistance device (PTAMR device) is fabricated. A schematic illustration of the experimental set-up is shown in **Figure 2a**. Photolithography and Ar ion etching are used to pattern Hall bars from the film. E-beam evaporation together with a liftoff process is used to form the contact electrodes. The fabricated device is then coated with 10 nm SiO₂ as a protective layer. Red-light (660 nm) illumination of 0.5 W/cm² is used to trigger the phase-transition.^{34–36} Magnetic field applied in-plane along the current direction is defined as H_x , and perpendicular is defined as H_y . The magnetic and transport characteristics is studied via the magnetoresistance effect. **Figure 2b** shows the optical and microscopic images of this device. The width and length of typical wires we test in this work are 3 μm and 50 μm , respectively. The magnetoresistance curves measured with H_x field applied are shown in **Figure 2c & 2d**. The resistance drops more than 10% with illumination applied, which can be caused by the phase-transition of VO₂ from insulator to metal. Another obvious variation in this process is that the coercivity changes from about 50 Oe to less than 10 Oe. After excluding the influence of thermal effect (**Supplementary Fig. S2c**), this feature reflects the alteration in the coercive field and/or the magnetic anisotropy.

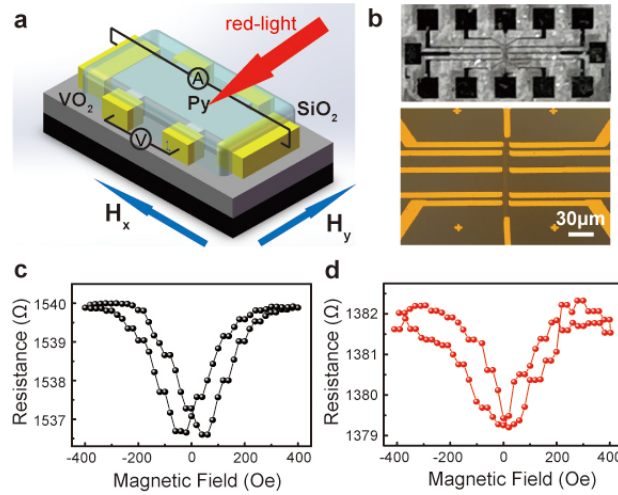


Figure 2 | PTAMR devices and magnetoresistance measurements. (a) Schematic drawing of the PTAMR devices. Direction of the applied magnetic fields H_x and H_y are also present. (b) Optical and microscopic images of the device. (c & d) Comparison of the H_x magnetoresistances of NiFe (5 nm)/VO₂ (40 nm)/TiO₂ (100) device without (c) and under (d) the illumination of 0.5 W/cm² red-light.

This modulation effect enables multi-field control of the resistance in the device, which can also benefit corresponding applications. **Figure 3a & 3b** show that the magnetoresistance curves of the heterostructure system would move to a lower resistance state if the illumination is applied, owing to that VO₂ could play as a current distribution layer in the process of phase-transition. Utilizing this feature, the PTAMR device provides an opportunity to achieve multi-resistance states, under multiple controls of the magnetic field and light illumination. **Figure 3c** demonstrates an example of six different resistance states, realized via synergistic control of light illumination and magnetic field. Both the field control and illumination control feature a reversible, repeatable and stable modulation on the device resistance. Limited by the nature of AMR effect, the change rate is just around 10^{-3} . Further transplantation of this phase-transition spintronic effect into other systems like GMR or TMR would realize similar but more appreciable performance, which would promote the development of high-density storage via multi-state memory.

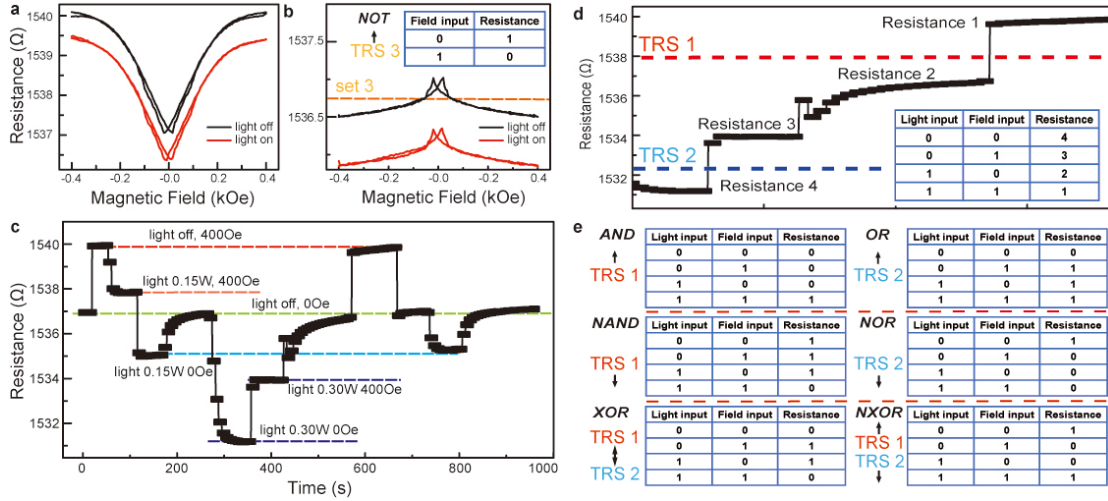


Figure 3 | Multi-resistance states and programmable logic implementation. (a & b) Magnetoresistance curves measured with the power of 0.15 W/cm^2 red-light illumination on and off. The magnetic field is applied in (a) H_x and (b) H_y direction. (c) Six different resistance states are realized using two kinds of illumination power, and 400 Oe H_x magnetic field. (d) Four resistance states are picked out from (c) to illustrate the logic operation. Light and magnetic field are designed as two kinds of input signals, which means illumination off (400 Oe) is set as logic 1 and on (0 Oe) as logic 0, while field applied (400 Oe) is set as logic 1 and removed (0 Oe) as logic 0. The result is read out by the resistances and shown in the truth table. Two threshold resistances setting (TRS) are marked as red and blue dash line. (e) The truth table of six basic logic operations with different TRSs. The arrow shows in which resistance range the signal should be picked as 1, and the opposite ought to be 0. NOT operation can be achieved by turning the field to H_y with the same setting of the field input. The threshold voltage and truth table are shown alone in (b).

As we know, optical devices have the characteristics of high-speed, high-bandwidth and low-loss, while traditional spintronic devices have the characteristics of non-volatile, high-speed and low-power-consumption. In this sense, an emerging device which could respond to both optical and Oersted-field inputs would be promising for next-generation electronics. In the following, we will present a demonstration of multi-field programmable logic gates based on the PTAMR device. **Figure 3d** gives four resistance states which are picked out from Figure 3c corresponding to a light illumination of 0.3 W/cm^2 . The programmable logic gates

include two kinds of inputting signals: light and magnetic field, which carry the input logic information. The light input with illumination on and off are defined as input 0 and input 1, respectively. While, field input with magnetic field applied (400 Oe) and removed (0 Oe) are set as input 1 and input 0, respectively. The computation is read out by measuring the resistances.

As illustrated in the truth table in **Figure 3d**, four different resistance states can be achieved with different inputs. In this case, we can set different threshold resistances to define in which range the resistance can be read out as logic 1 and in which as logic 0. Two threshold resistance settings (TRSs) have been marked as dashed line in **Figure 3d**. **Figure 3e** illustrates how to implement six basic universal Boolean logic functions in a single phase-transition spintronic device. Taking AND for example, it is a logic function of two binary inputs, where the output is always logic 0, except for the inputs being both logic 1, in which case the output is logic 1. TRS 1 is used in this case. Output resistance above TRS 1 is defined as logic 1, and resistance below is logic 0, which means resistance 1 (R1) is logic 1, and resistance 2 (R2), 3 (R3) and 4 (R4) are logic 0. As a result, for input with illumination on and field removed, the output is 0. So as the operation of illumination on and field applied or illumination off and field removed. Only when the input of illumination off and field applied is both given, then the logic 1 is outputted. Detailed settings of this phase-transition device to realize different logic functions have been present in Figure 3e. The arrow shows in which resistance range the signal should be picked as 1, and the opposite ought to be 0. Following the instructions of the arrows in **Figure 3e**, logic functions of OR, NAND and NOR can be fulfilled. For the case of XOR and NXOR, TRS 1 and TRS2 are both used to define the resistance range. If the resistance between TRS 1 and TRS2 is logic 1, and exceeded is logic 0, then we get R2, R3 to be logic 1, and R1, R4 to be logic 0. So XOR is programmed. If the setting is reversed, NXOR is programmed. For the case of NOT logic operation, light input can be omitted. The logic can be achieved by turning the field from H_x to H_y direction with the same setting of the field input (**Figure 3b**). This phase-transition spintronic device, which could achieve varieties of logic functions in a single device, has great application potential in the reconfigurable, programmable and cascable

logics beyond CMOS, and will pave a way for big data and neuromorphic computing.^{37,38}

Strain analysis and mechanism discussion

To clarify the relationship between magnetism modulation and interfacial strain, substrates with different crystal surface is used to contrast the modulation effect. **Figure 3a** gives the schematic illustration of the heterostructures and the analysis of the crystal axis conversion of VO₂ in the phase-transition from monoclinic to rutile.³⁹ The structure variation of VO₂ was qualitatively analysed based on the bulk parameters (see details in **Supplementary Table S1**).²⁷ On TiO₂ (001) substrate, the in-plane lattice constant changes are around 0.4% and 0.2% along a_R and b_R direction (**Figure 4b**). On TiO₂ (100) substrate, the lattice constant is compressed about 0.8% alone c_R , and the change rate between b_R and c_M reaches 18.5% as shown in **Figure 4c**. In addition, there is a shear force caused by the angle decrease of β from 122.6° to 90°. As a result, the interfacial strain on TiO₂ (100) substrate should be much stronger than on TiO₂ (001) substrate.

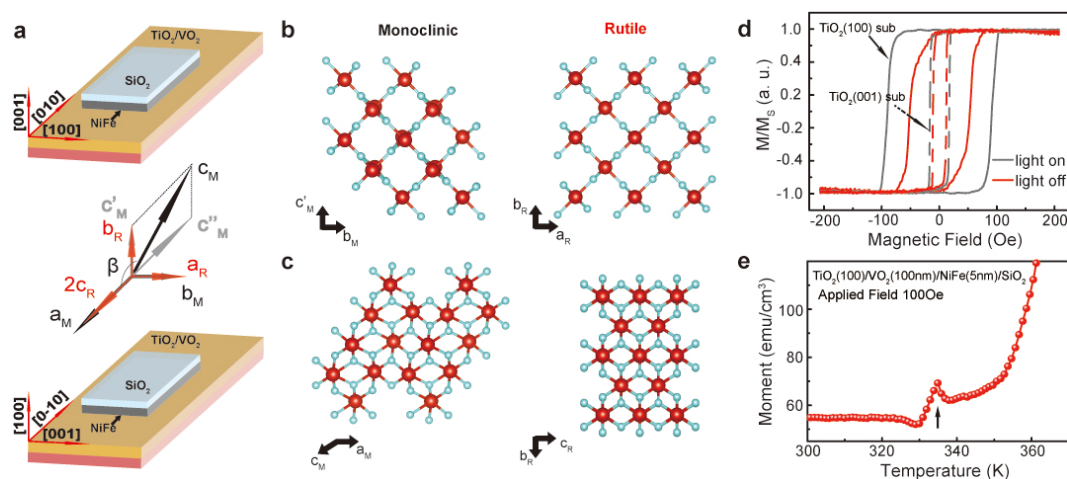


Figure 4 | Interface strain analysis and characterization of magnetism modulation. (a) Strain analysis of the interface between VO₂ and NiFe when the phase-transition of VO₂ happens. (b & c) Schematic diagram of the crystal lattice change of the (001) plane and (100) plane as regard to rutile structure. (d) Longitudinal Kerr signals of the NiFe/VO₂ heterostructure grown on different substrates. The H_C change rate between the red-light illumination on and off is 45% for TiO₂ (100)

substrate and 25% for TiO₂ (001) substrate respectively when the power of the illumination reaches 2 W/cm². (e) Temperature dependence of out-of-plane magnetization at magnetic field 100 Oe, the arrows correspond to VO₂ phase-transition temperature.

In-situ longitudinal magneto-optic Kerr effect (MOKE) measurements are carried out using red-light illumination as heat source for the samples deposited on TiO₂ (100) and (001) substrates. As illustrated in **Figure 4d**, it is found that the change rate of coercive field reaches 45% for TiO₂ (100) but only 25% for TiO₂ (001) sample during the transition of VO₂, which agrees with the interfacial strain analysis above. Further evaluations of heterostructures with different thicknesses of NiFe (**Supplementary Fig. S2a & S2b**) show that the change rate of H_C reaches 67% when the thickness decreases to 3nm, while quickly drops to almost 0% when the thickness increased to 10 nm. This is coordinated with the reports that magneto-elastic coupling coefficient of NiFe is anomalously large for thickness below 5 nm.⁴⁰ The thickness dependence feature and the MOKE analysis, together with the evidence excluding contributions of thermal effect (**Supplementary Fig. S2c**), thus verify that the interfacial strain coupling plays a crucial role in the magnetism modulation.

To further confirm that the magnetism variation is indeed related to the phase-transition of VO₂, we measured the temperature dependence of the magnetization. With the phase-transition, a magnetization increasing should be detected owing to the coercive field shrinking. As illustrated in **Figure 4e**, an abnormal peak can be detected in the M-T curve around the phase-transition temperature of VO₂, followed by an abrupt increasing of the magnetization which cannot be detected in a reference NiFe (5 nm) sample grown on SiO₂ substrate. With these experimental results, a conclusion could be drawn that the magnetism modulation during phase-transition of VO₂ is mainly attributed to the interfacial strain coupling of the heterostructure system.

Based on the understanding that the magnetism modulation is mainly attributed to the interfacial strain, we now focus on the variation of magnetic layer during the phase-transition to explain the origin of the magneto-elastic coupling.⁴¹ Recent research has shown that by engineering the surface, instead of staying in-plane, perpendicular or

other direction of magnetic anisotropy can be achieved in ultrathin magnetic films.⁴² In our phase-transition heterostructure system, the lattice variation in specific plane is quite large, which could probably lead to some periodic bending and spin reorientation of NiFe film in the interface region (**Supplementary Fig. S3a**).⁴³ Assuming that the main modulation mechanism in our films is domain wall motion, the coercivity H_C should depend on the pinning site of the domain wall which is characterized by a local minimum energy. It can be written as:⁴⁴

$$H_C \approx (\partial\gamma/\partial x)_{max}/(2\mu_0 M_S),$$

where x is the position of the domain wall, M_S is the saturation magnetization, μ_0 is the permeability in vacuum and γ is the domain wall energy. γ can be further written as:⁴⁵

$$\gamma = 4\sqrt{A(K_1 + \lambda_S\sigma)},$$

where A is the exchange constant, K_1 is the crystal anisotropy, λ_S is the magnetostriction coefficient and σ is the applied strain to the sample. So γ depends on σ and answers the origination of the magneto-elastic coupling. A possible description of this phenomenon is that the increased interface roughness may make the spin which originally pinned in-plane tend to turn to the direction out-of-plane⁴⁰ (**Supplementary Fig. S3b**). This is consistent with the experimental results of the increased K_u and enhanced squareness of the hysteresis loop out-of-plane after the phase-transition happens. As to the saturation magnetization decreasing and coercive force shrinking, it is probably caused by the varied distance between individual magnetic grains caused by the bending interface structure. The inter-granular interaction might be crippled, which decreases the intrinsic spin flipping barrier and long-range magnetostatic coupling.

Conclusions

In summary, we have demonstrated the phase-transition induced electronic and magnetic modulation in the NiFe/VO₂ bilayer heterostructure. Multi-field induced changes in the conductivity (10%), coercivity (60%), saturation magnetic strength (7%) and magnetic anisotropy (33.5%) are observed during the phase-transition. The increase of interfacial magnetic anisotropy, from 0.755 to 0.885 erg/cm², shows a potential to induce perpendicular magnetic anisotropy. Further research about the phase-transition

AMR device fabricated by the heterostructure sample shows that multi-state resistances and seven basic logic functions (AND, OR, NAND, NOR, XOR, NOT and NXOR) can be achieved in a single device. Theoretical analyses and the experiment evidences reveal that the magneto-elastic coupling at the interface induced by appreciable interfacial strain (up to 18.5%) may be the origin of magnetism modulation. Our work, as a demonstration of phase-transition spintronics, may pave a way for next-generation electronics.

Methods

Heterostructure and device fabrication. The VO₂ thin films were grown on (001) and (100) TiO₂ substrates using a pulsed laser deposition (PLD) system (KrF, $\lambda=248$ nm). Growth of epitaxial VO₂ thin films was performed at 500 °C and 2.0 Pa of oxygen. The laser fluence and repetition rate were fixed at 4 J/cm² and 2 Hz, respectively. The film thickness was 40 nm after 7200 pulses of deposition. The Ni₈₀Fe₂₀ films were magnetron-sputtered at room temperature. Raw bilayer samples were then patterned by optical lithography (Micro Writer ML Baby, Durham Magneto Optics) followed by argon ion-beam etching into Hall bars with several legs of different spacing (Figure 2a&b). Optical lithography and e-beam evaporation were then used to prepare Cr (5 nm)/Au(100 nm) electrodes. 10nm SiO₂ was then deposited by thermal evaporation on the device as a protection layer.

Characterization and measurement. The magnetic properties were measured partly by MOKE (NanoMOKE3, Durham Magneto optics ltd) at room temperature and partly by SQUID (MPMS3, Quantum Design, Inc.) at room and high temperature. The phase-transition AMR devices were measured by normal 4-terminal methods with Keithley 6221 and Keithley 2182 sourcing and measuring units, respectively. Meanwhile, an in-plane electromagnet (East Changing Co. China) provided magnetic fields with proper directions.

References

1. Zeches, R. J. *et al.* A Strain-Driven Morphotropic Phase Boundary in BiFeO₃. *Science* **326**, 977–980 (2009).
2. Wang, J. *et al.* Epitaxial BiFeO₃ multiferroic thin film heterostructures. *Science* **299**, 1719–1722 (2003).
3. Ramesh, R. & Spaldin, N. A. Multiferroics: Progress and prospects in thin films. *Nat. Mater.* **6**, 21–29 (2007).
4. Spaldin, N. A. The Renaissance of Magnetoelectric Multiferroics. *Science* **309**, 391–392 (2005).
5. Chappert, C., Fert, A. & Van Dau, F. N. The emergence of spin electronics in data storage. *Nat. Mater.* **6**, 813–823 (2007).
6. Lei, N. *et al.* Strain-controlled magnetic domain wall propagation in hybrid piezoelectric/ferromagnetic structures. *Nat. Commun.* **4**, 1378 (2013).
7. Eerenstein, W., Wiora, M., Prieto, J. L., Scott, J. F. & Mathur, N. D. Giant sharp and persistent converse magnetoelectric effects in multiferroic epitaxial heterostructures. *Nat. Mater.* **6**, 348–351 (2007).
8. Cai, T. *et al.* Magnetoelectric coupling and electric control of magnetization in ferromagnet/ferroelectric/normal-metal superlattices. *Phys. Rev. B* **80**, 140415 (2009).
9. Wu, S. M. *et al.* Reversible electric control of exchange bias in a multiferroic field-effect device. *Nat. Mater.* **9**, 756–761 (2010).
10. Bauer, U. *et al.* Magneto-ionic control of interfacial magnetism. *Nat. Mater.* **14**, 174–181 (2015).
11. Li, H.-B. *et al.* Electric-field control of ferromagnetism through oxygen ion gating. *Nat. Commun.* **8**, 2156 (2017).
12. Stern, A., Dzero, M., Galitski, V. M., Fisk, Z. & Xia, J. Surface-dominated conduction up to 240 K in the Kondo insulator SmB₆ under strain. *Nat. Mater.* **16**, 708–711 (2017).
13. Zhu, Y., Withers, R. L., Bourgeois, L., Dwyer, C. & Etheridge, J. Direct mapping of Li-enabled octahedral tilt ordering and associated strain in nanostructured perovskites. *Nat. Mater.* **14**, 1142–1149 (2015).
14. Choi, K. J. Enhancement of Ferroelectricity in Strained BaTiO₃ Thin Films. *Science* **306**, 1005–

- 1009 (2004).
15. Lee, M. L., Fitzgerald, E. A., Bulsara, M. T., Currie, M. T. & Lochtefeld, A. Strained Si, SiGe, and Ge channels for high-mobility metal-oxide-semiconductor field-effect transistors. *J. Appl. Phys.* **97**, 11101 (2005).
 16. Boschker, H. *et al.* High temperature magnetic insulating phase in ultrathin $\text{La}_{0.67}\text{Sr}_{0.33}\text{MnO}_3$ films. *Phys. Rev. Lett.* **109**, 157207 (2012).
 17. Llordés, A. *et al.* Nanoscale strain-induced pair suppression as a vortex-pinning mechanism in high-temperature superconductors. *Nat. Mater.* **11**, 329–336 (2012).
 18. Sander, D., Enders, A. & Kirschner, J. Stress and magnetic properties of surfaces and ultrathin films. *J. Magn. Magn. Mater.* **200**, 439–455 (1999).
 19. Sander, D. The correlation between mechanical stress and magnetic anisotropy in ultrathin films. *Reports Prog. Phys.* **62**, 809–858 (1999).
 20. Pryce, I. M., Aydin, K., Kelaita, Y. A., Briggs, R. M. & Atwater, H. A. Highly Strained Compliant Optical Metamaterials with Large Frequency Tunability. *Nano Lett.* **10**, 4222–4227 (2010).
 21. Nan, T. *et al.* Quantification of strain and charge co-mediated magnetoelectric coupling on ultrathin Permalloy/PMN-PT interface. *Sci. Rep.* **4**, 3688 (2015).
 22. Liu, M., Lou, J., Li, S. & Sun, N. X. E-Field Control of Exchange Bias and Deterministic Magnetization Switching in AFM/FM/FE Multiferroic Heterostructures. *Adv. Funct. Mater.* **21**, 2593–2598 (2011).
 23. Song, C., Cui, B., Li, F., Zhou, X. & Pan, F. Recent progress in voltage control of magnetism: Materials, mechanisms, and performance. *Prog. Mater. Sci.* **87**, 33–82 (2017).
 24. Imada, M., Fujimori, A. & Tokura, Y. Metal-insulator transitions. *Rev. Mod. Phys.* **70**, 1039–1263 (1998).
 25. Dagotto, E. Complexity in Strongly Correlated Electronic Systems. *Science* **309**, 257–262 (2005).
 26. Nakano, M. *et al.* Collective bulk carrier delocalization driven by electrostatic surface charge accumulation. *Nature* **487**, 459–462 (2012).
 27. Paorici, C. *et al.* The mechanism of electrical threshold switching in VO_2 crystals. *J. Phys. C Solid State Phys.* **13**, 5725–5733 (1980).
 28. Lee, S. *et al.* Anomalously low electronic thermal conductivity in metallic vanadium dioxide.

- Science* **355**, 371–374 (2017).
29. Jeong, J. *et al.* Suppression of Metal-Insulator Transition in VO₂ by Electric Field-Induced Oxygen Vacancy Formation. *Science* **339**, 1402–1405 (2013).
 30. Liu, K., Lee, S., Yang, S., Delaire, O. & Junqiao, W. Recent progress on physics and applications of VO₂. *Mater. Today* in press (2018).
 31. Wang, W. G., Li, M., Hageman, S. & Chien, C. L. Electric-field-assisted switching in magnetic tunneljunctions. *Nat. Mater.* **11**, 64–68 (2012).
 32. Ikeda, S. *et al.* A perpendicular-anisotropy CoFeB–MgO magnetic tunnel junction. *Nat. Mater.* **9**, 721–724 (2010).
 33. Engel, B. N., England, C. D., Van Leeuwen, R. A., Wiedmann, M. H. & Falco, C. M. Interface magnetic anisotropy in epitaxial superlattices. *Phys. Rev. Lett.* **67**, 1910–1913 (1991).
 34. Ma, H. *et al.* Flexible, All-Inorganic Actuators Based on Vanadium Dioxide and Carbon Nanotube Bimorphs. *Nano Lett.* **17**, 421–428 (2017).
 35. Xiao, L. *et al.* Fast Adaptive Thermal Camouflage Based on Flexible VO₂/Graphene/CNT Thin Films. *Nano Lett.* **15**, 8365–8370 (2015).
 36. Dong, K. *et al.* A Lithography-Free and Field-Programmable Photonic Metacanvas. *Adv. Mater.* **30**, 1703878 (2018).
 37. Xia, Q. *et al.* Memristor-CMOS Hybrid Integrated Circuits for Reconfigurable Logic. *Nano Lett.* **9**, 3640–3645 (2009).
 38. Coskun, A., Deniz, E. & Akkaya, E. U. Effective PET and ICT switching of boradiazaindacene emission: A unimolecular, emission-mode, molecular half-subtractor with reconfigurable logic gates. *Org. Lett.* **7**, 5187–5189 (2005).
 39. Tao, Z. *et al.* Decoupling of structural and electronic phase transitions in VO₂. *Phys. Rev. Lett.* **109**, 166406 (2012).
 40. Song, O., Ballentine, C. A. & O’Handley, R. C. Giant surface magnetostriction in polycrystalline Ni and NiFe films. *Appl. Phys. Lett.* **64**, 2593–2595 (1994).
 41. Reekstin, J. P. Zero Magnetostriction Composition of NiFe Films. *J. Appl. Phys.* **38**, 1449–1450 (1967).
 42. Tretiakov, O. A., Morini, M., Vasylykevych, S. & Slastikov, V. Engineering Curvature-Induced Anisotropy in Thin Ferromagnetic Films. *Phys. Rev. Lett.* **119**, 77203 (2017).

43. Graczyk, P., Schäfer, R. & Mroz, B. Magnetoelastic coupling between NiFe thin film and LiCsSO₄ studied by Kerr microscopy. *J. Phys. D: Appl. Phys.* **48**, 425002 (2015).
44. Garshelis, I. J. Force transducers based on the stress dependence of coercive force. *J. Appl. Phys.* **73**, 5629–5631 (1993).
45. Garrett, C. *et al.* Thickness dependence of the magnetic hysteresis of NiFe-31% films as a function of an applied isotropic in-plane stress. *J. Appl. Phys.* **93**, 8624–8626 (2003).

Acknowledgments

This work was supported by the National Natural Science Foundation of China (Nos. 51602013, 61704005, 61571023 and 61627813), the International Collaboration 111 Project (No. B16001), Beijing Natural Science Foundation (No. 4162039) and funding support from Beijing Advanced Innovation Center for Big Data and Brain Computing (BDBC). The authors thank Jiwei Hou, Runrun Hao, Chen Cai, Xiaofei Fan and Yuan Cao for the help during the device fabrication.

Author contributions

G.D.W. and X.Y.L. contributed equally to this work. X.Y.L. and W.S.Z. coordinated the project. X.Y.L. proposed and designed the research. G.D.W., Z.Z.S., D.W., X.H.W., K.L.J., K.L. and Y.X.C. performed the sample preparation. G.D.W., Z.Z.S. and X.Y.L. performed the heterostructure characterization and measurement. Z.H.W., G.D.W. and X.Y.L. performed the micromagnet simulation. G.D.W., Z.Z.S. and X.Y.L. performed the device fabrication and measurement. G.D.W., X.Y.L., Y.X.C. and W.S.Z. contributed to the mechanism interpretation. G.D.W., X.Y.L. and W.S.Z. wrote the paper. All the authors participated in discussions of the research.

Competing interests

The authors declare no competing interests.

Additional information

Supplementary Information is available for this paper at [http:// www.nature.com/ncomms/](http://www.nature.com/ncomms/)